Engineering Notes

Numerical Investigation of Wind-Tunnel Model Deformations Caused by the Twin-Sting Support System

Roberto Flores,* Enrique Ortega,† and Eugenio Oñate‡
International Center for Numerical Methods in Engineering,
Universidad Politécnica de Cataluña,
08034 Barcelona, Spain

I. Introduction

THE present work is part of a broader investigation aimed at improving the understanding of the aerodynamics of the rear aircraft section. Complex flow phenomena (e.g., the thick fuselage boundary layer at the rear end) present a challenge to the accurate predictions of aerodynamic performance. Significant efficiency gains are expected from improved-fidelity computations and experimental techniques. As part of a joint effort between several research institutions and industrial partners, a series of wind-tunnel test campaigns focusing on accurate rear-end measurements was planned. To obtain accurate tail-force data, a nonstandard *live-rear-end* test model was adopted. This technique uses a mechanically separate rear-end section attached to the main body through internal balances, allowing direct measurement of the force acting on the tail. This mechanical setup precludes the use of a conventional tail-cone-attached sting. Moreover, to minimize aerodynamic interference on the empennage caused by the support system, a wing-attached twin-sting mounting was chosen (see Fig. 1).

Two series of test campaigns were programmed. The first campaign targeted the low-Reynolds-number regime to be performed at the Aircraft Research Association conventional transonic wind tunnel. The second campaign aimed at true cruise Reynolds numbers and was planned at the pressurized cryogenic facility of the European Transonic Windtunnel. The same test model, with only minor modifications, was employed in both campaigns.

Although the direct aerodynamic interference from the booms is reduced by moving them away from the tail section, additional stresses are introduced in the wings that alter their mechanical behavior. A certain number of papers in existing literature focus on the aerodynamic interference effect of the twin stings: for example, [1,2]. On the other hand, the number of published studies dealing with the aeroelastic effects is surprisingly small. To the best of the authors' knowledge, most of the information available comes from indirect experimental measurements [3,4], with no systematic numerical study having been published. If accurate aerodynamic measurements are to be obtained, the possible perturbations due to wing deformation when using the twin-sting arrangement must be

explored. Changes in wing twist modify the spanwise lift distribution and therefore, through modified downwash, affect the tail flowfield. Although the importance of this effect is widely acknowledged by the experimental aerodynamicists, the amount of effort allocated in the past to its investigation is very modest. The present study aims at filling this gap by improving the understanding of the differences in structural behavior between a model supported by the fuselage and a twin-sting mounted model. This information is necessary to determine the limitations of the experimental technique and increase confidence in the measurements. Although it is desirable from the strictly aerodynamic point of view to place the stings as far apart as possible (to distance them from the tail section), the increased separation might entail larger wing deformations, thus negatively impacting the measurements. As a first step toward achieving an optimal compromise between these effects, it is necessary to carry out a detailed study of wing deformations as a function of the different test setup characteristics. In particular, the changes caused by variations of the boom spacing must be investigated (the published results cover only one value of the distance for each test model and therefore do not provide information on its effect). This Note focuses on the study of wing model deformation due to the twin-sting support mechanism, with an emphasis on wing torsion and bending. Using numerical simulation of both the flowfield and the structural response, the model deformations encountered during wind-tunnel testing have been predicted. A parametric study has been performed to assess the changes in shape over the complete test envelope (including flight conditions as well as sting spacing effects). Although the focus is on structural behavior, the results are also meant to be used at a later stage to modify computational fluid dynamics (CFD) meshes and to thus improve numerical drag predictions.

The work is organized as follows. The aerodynamic model is described in Sec. II, with the structural model and coupling scheme following in Sec. III. A parametric study of wing deformation is presented in Sec. IV. Finally, the most relevant conclusions of this work are summarized in Sec. V.

II. Aerodynamic Modeling

A. Model Geometry and Discretization

The analysis geometry involves a wing–body–tail test-model configuration supported by twin stings. The shape corresponds to a modern large jetliner. The 1:50-scale model has a half-span of 79 cm. In the present work, three different support configurations have been analyzed to evaluate their effect on model deformation. These shall be referred to as outboard, intermediate, and inboard boom positions. The respective sting spacings are 43, 35, and 30 in., corresponding to 69, 56, and 48% spanwise positions (this choice of values allowed the reuse of an existing yoke plate, thus saving costs). All of them have been tested during the conventional (i.e., noncryogenic) wind-tunnel test campaign. Some cryogenic-wind-tunnel entries were also scheduled using the intermediate spacing. The outermost boom position was chosen based purely on the allowable material stresses and is meant to provide an upper limit on the aeroelastic deformations. The intermediate position is representative of standard experimental practice, and the smallest boom spacing was selected to gain understanding on the interference effects over the empennage caused by the twin-sting arrangement. Because of the fact that flow conditions and geometry are symmetric with respect to the aircraft midplane (x–z), a half-symmetric computational model is used. Figure 2 shows the test-model geometry and the different sting positions studied here.

As Fig. 2 shows, the full assembly of the wind-tunnel support system has not been modeled (the yoke plate and boss have been removed). To simplify the geometry, only the stings have been

*Postdoctoral Researcher, Aerospace Department, Edificio C1, Campus Norte, Gran Capitán.
†Research Staff, Aerospace Department, Edificio C1, Campus Norte, Gran Capitán.
‡Director, Edificio C1, Campus Norte, Gran Capitán.

Fig. 1 Photograph of a wind-tunnel test model suspended with twin stings.
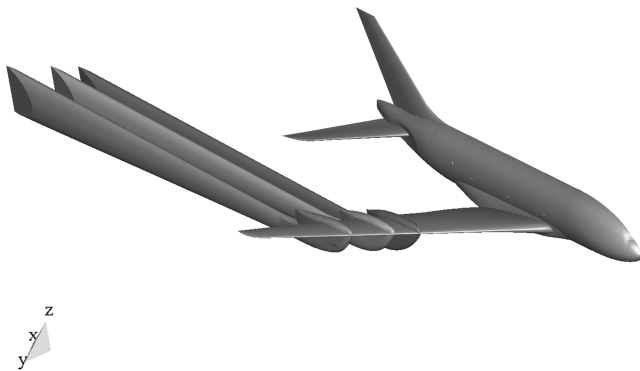

Fig. 2 Test model showing the three boom spacings tested.

considered. The rear part of the booms has been streamlined to minimize the disruption of the flow pattern. The resulting computational model offers substantial savings in both meshing effort and CPU runtime requirements. An unstructured tetrahedral mesh containing approximately ten million elements has been generated from the relevant CAD geometries. Although this might seem to be an excessive grid resolution just for structural calculations, obtaining acceptable-quality aerodynamic data was necessary, because it was used in a separate study of aerodynamic interference effects at the horizontal tail plane (HTP). Given the relative magnitude of the different aerodynamic forces acting on the structure, it is apparent that the viscous shear stresses are small compared with the pressure differences encountered. Moreover, the wing bending moment caused by the viscous stresses acts approximately around the model z axis (vertical), for which the wing stiffness is highest. Consequently, it can be safely assumed that most of the wing structural deformation is caused by the pressure field, with viscous forces playing a negligible role. Hence, the fluid has been considered inviscid, allowing for considerable computational savings (for the flight regimes analyzed, no large separation areas appear, and so the Euler equations provide a good approximation to the real flowfield).

B. Flow Solver

Because of the complexity of the geometries to be analyzed, the ability to use unstructured grids was an important design consideration. An in-house finite element unstructured Euler solver has been thus developed. Moderate run times in modest hardware were also sought. To fulfill these requirements, an edge-based data structure [5] was chosen over the more conventional element-based storage scheme. The solver is stabilized using Roe's approximate Riemann solver [6] combined with a MUSCL variable-order-limited extrapolation scheme [7] to achieve up to third-order space accuracy

of the interface fluxes. To improve behavior in modern hardware, the code has been optimized for running in shared-memory parallel architectures using OPEN-MP directives. Care has also been taken to minimize memory access overheads by reducing cache misses through appropriate reordering of memory contents and sequencing of data accesses [8].

III. Structural Modeling

The experimental model has been manufactured to meet the requirements of testing in a pressurized cryogenic environment. It must be capable of withstanding an increased dynamic pressure (when compared with conventional wind-tunnel testing) while providing acceptable geometrical stability. The material must also retain its mechanical properties at liquid-nitrogen temperatures. To this effect, a high-strength maraging steel has been chosen with a Young's modulus of 181 GPa and a Poisson's ratio of 0.3. A finite element structural model has been developed to analyze the deformations caused by the aerodynamic loads. An overview of the structural modeling of the model aircraft, the support system, and the fluid–structure coupling procedure adopted is presented next.

A. Wing Structural Model

A 3-D model of the wing structure has been developed to assess the changes in twist and bending caused by the twin-sting mounting arrangement. Calculations have been performed using the commercial finite element code ABAQUS. For structural modeling purposes, the wing has been considered to be solid. The size of the cavities necessary to route the measuring equipment has been kept to the absolute minimum to preserve the stiffness of the model. Therefore, the behavior of the wing can be approximated successfully by neglecting the effect of the internal holes. If the highest level of accuracy is sought in the calculations, a structural mesh containing only well-shaped hexahedral elements should be used. However, this is difficult to achieve using only brick-type elements, especially on the area surrounding the leading edge. The higher curvature of this region (especially near the wing tip) would cause some elements to warp beyond acceptable levels. To circumvent this problem, a hybrid mesh, hexahedral-dominant but containing some triangular prisms on the leading edge, has been adopted. This way, most of the wing is modeled with well-shaped structured hexahedral elements, and the distortion problems near the leading edge are alleviated by the prismatic elements. The wing structural mesh contains 49,358 nodes shared by 6160 prisms and 40,000 brick (hexahedral) elements.

Fully integrated linear elements subject to bending tend to show an excessive stiffness, due to their inability to reproduce a linearly varying strain field without developing parasitic shear stresses [9]. It is therefore advised to use second-order elements to avoid shear locking problems. Unfortunately, as the wing section tapers toward the tip, the elements become severely skewed (especially at the leading edge, as it curves backward over a very short distance). Second-order elements suffer considerable performance degradation under these circumstances and can lead to severe convergence problems (caused by the Jacobian of the isoparametric transform becoming negative). To overcome this difficulty, it was decided to employ first-order (linear interpolation) elements, as their behavior is less sensitive to distortion. To prevent the mesh from developing shear locking, enhanced-strain-field linear elements have been used. These elements include additional incompatible displacement modes that prevent spurious shear stresses. To double-check the results, tests have also been performed using reduced-integration elements. These do not suffer from shear locking, as no strain develops at their integration points when subject to pure bending. However, this circumstance allows unrestricted growth of certain displacement combinations (the so called zero-energy or hourglassing modes). To prevent propagation of these spurious modes, hourglass control [10] is included. An extra component of strain energy is associated with the amplitude of the zero-energy modes, restricting their propagation and avoiding detrimental effects on accuracy. No significant differences in behavior have been observed between the two different

element formulations, and so the results can be considered to be reliable.

B. Support Mechanism Modeling

Large vertical displacements along the model z axis and rotations along the y axis (spanwise direction) are to be expected, due to the bending deformation of the booms. The effects of displacements of the supporting mechanism on the measurements carried out during testing are quite limited, because model attitude is measured via inclinometers mounted on the fuselage. Therefore, the fuselage incidence is always set to the correct value, irrespective of the level of deformation experienced by the booms. Nevertheless, boom stiffness must be properly accounted for to obtain realistic wing-deformation predictions. There is an important coupling caused by the torsional stiffness of the booms, which restricts the rotation of the wing around the x axis (fuselage direction) and therefore hampers bending deformation. To reduce the complexity of the model while still retaining this coupling effect, the stings have been modeled using beam elements. The bending and torsional stiffness of the beams has been calculated from the detailed CAD model of the booms.

The wing–boom adaptors consist of two massive steel parts bolted together with the wing clamped in between. Given their general proportions, the adaptors have been modeled as rigid, as their stiffness is much higher than that of the booms and the wing section. The realistic simulation of the adaptor–wing junction would require a very detailed modeling of the attachment mechanism to produce an accurate rendering of the stress field around the load-transfer area (including, for example, information about the bolt-adjustment torque). To avoid unnecessary complexity, the model has been simplified in this area. The load from the adaptors has been transferred to the wing by rendering a group of elements around the fasteners extremely rigid and constraining their movements to those of the adaptor. This way, the load transfer is spread out over several elements producing a locally smooth deformation field.

C. Body–Tail Section Modeling

The fuselage diameter is very large compared with the wing thickness, therefore its deformations are very small compared with those of the wing. Moreover, the deformations sought are those of the wing so the computational complexity has been reduced by removing the body–tail assembly from the structural mesh. To this effect, the overall pressure load acting on the body–tail assembly has been reduced to a point force and moment about the wing mean aerodynamic center. Hence, the effects of the body–tail group are accounted for without increasing the number of degrees of freedom in the model.

D. Modeling of the Body–Wing Interface

The load-transfer mechanism at the wing root depends on the geometrical details of the junction (e.g., on the type and distribution of fasteners). A detailed model of the interface was not considered necessary as the stiffness of the wing is maximum in this area (due to the large chord and thickness). Therefore, most of the expected displacements arise from the deformation of sections farther away from the fuselage. Moreover, the wing–fuselage junction is covered by the belly fairing (which is a separate component of the test model), so the local behavior of the underlying structure has a very limited impact on the external shape. In the simplified approach adopted a group of elements on the upper and lower sides of the wing root (six along each) has been lumped into a single rigid body. The master reference node (the node to which the displacements of all the nodes in the rigid body are tied to) is the reduction point of the fuselage–tail aerodynamic loads (i.e., the mean aerodynamic center). This way, the rotations of the wing root section and the fuselage are constrained to remain equal, whereas a certain level of warping is allowed for the wing (fully constraining the warping of the section could give rise to an unrealistic torsional stiffness at the wing root). Note that this form of attachment can be considered similar to spot-welding the wing root to the fuselage body. Furthermore, x–z symmetry conditions for

the model are enforced constraining the motion of the body–tail reference node along the y axis as well as the rotations about the x and z axes. Thus, the effects of the body–tail assemble on the wing are reproduced in a very computationally effective way.

E. Transfer of the Aerodynamic Loads to the Structural Model

As the fluid and solid grids are not congruent, an automated method to map the pressure distribution from an arbitrary CFD grid into the structural mesh has been developed. This load transfer procedure is carried out in four main steps:

1) The CFD surface mesh is split in two groups, the first one containing elements belonging to the body–tail area and the second one including all the remaining surface facets.

2) The pressures acting on the body and tail are reduced to a global force and moment acting on the reference point.

3) For each surface facet of the structural grid, the centroid is calculated and the element of the CFD mesh it lays on is sought.

4) The average pressures at the centroids of the structural mesh facets are interpolated using values from the elements of the CFD grid on which they are located. These pressures are subsequently converted to nodal generalized forces of the solid model.

The third step of the process could be extremely lengthy if a brute-force approach were used to find the correspondence between the fluid and the structural grids. For a CFD grid containing n_c facets and a structural mesh having n_s surface elements, a total of $n_c \times n_s$ checks would have to be performed. It is clear that this is an extremely inefficient process that calls for improvement. To achieve this, a *binning* algorithm has been implemented [8]. A background, uniformly spaced, hexahedral structured mesh is created that encompasses the complete wing. In the first step, the CFD facets are assigned to the elements of the background mesh (the bins) according to the position of their centroids. Given the uniform spacing of the bins, the parent bin of any point can be located by simply operating on its coordinates, and the process is thus extremely fast. In the second step, the underlying fluid element of each structural face is found by searching only across the elements belonging to the same bin. The cost of the search is then reduced by a factor equal to the number of elements on the background mesh. As the number of bins can be made as large as needed, the speedup attained is quite remarkable.

F. Coupling Procedure

The pressure distribution obtained from the CFD solution is converted to nodal generalized forces applied on the structure, but the displacements and rotations thus obtained are not used to deform the aerodynamic model and recalculate the pressure forces. No iteration between the CFD and the structural model is performed and, consequently, the static aeroelastic equilibrium of the wing is not achieved. As the structure of the test model is very stiff (making the displacements small), neglecting the effect of the deformations on the flowfield does not lead to severe errors (from the structural point of view). To validate this assumption, a cross-check has been made against experimental deformation data gathered during cryogenic-wind-tunnel testing. A limited set of direct displacement measurements using the image pattern correlation technique (IPCT) and stereo pattern tracking (SPT) were available for comparison. Both techniques are based on photogrammetric principles [11,12]. In SPT a regular array of spot markers is tracked, whereas IPCT relies on randomly sprayed paint droplets. By comparing images of the markers taken from different points of view, their 3-D coordinates can be inferred, thus allowing determination of the displacements. The experimental measurements cover only the intermediate boom spacing and therefore do not provide a great insight on the effect of sting position. They are, however, useful as a means to validate the numerical approach.

Using the methodology outlined in the previous sections, a prediction of the wing twist deformation encountered during cryogenic testing was made. The good agreement between the numerical and experimental results is shown in Fig. 3. The general trend (as well as the actual rotation values) is well-captured. It must be stressed that
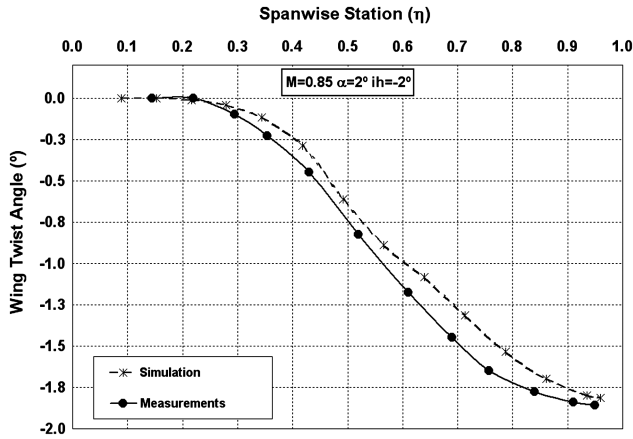
Fig. 3 Simulated vs experimental wing twist; $M_\infty = 0.85$. $\alpha = 2°$, midboom position, and HTP incidence setting = $-2°$.

the differences seen on the graph are of limited relevance. During testing, discrepancies on the order of 10% were sometimes observed between the SPT and IPCT measurements. Thus, the differences in Fig. 3 may be due to experimental uncertainties. The *one-way coupling* procedure adopted in this work then seems very accurate.

IV. Wing Deformation Analysis

In this section, the influence of the angle of attack on wing deformation is analyzed for the different sting spacings. All the results presented here correspond to a fixed Mach number of 0.85, representative of cruise conditions. Keeping the Mach number constant removes some purely aerodynamic effects from the analysis (for example, the corresponding changes in the dynamic pressure inside the test chamber) and simplifies the interpretation of the results. To transform the C_p values obtained from the CFD solution into pressure loading, a constant stagnation pressure of 1 bar is assumed to match the test-chamber conditions encountered during the conventional wind-tunnel runs.

To assess the effects of the mounting system on wing deformation, two parameters have been investigated. The first one is the rotation angle about the y axis of the wing sections (also termed twist angle). This parameter is considered to be the most relevant result from the structural analysis, because it represents the local change in angle of attack due to aeroelastic effects and has a major impact on the downwash distribution at the tail. For each of the cases under study, the twist angle has been computed at several spanwise stations in the following manner:

$$\text{twist angle} = \tan^{-1}\left(\frac{u_Z^{LE} - u_Z^{TE}}{x^{LE} - x^{TE}}\right) \qquad (1)$$

where u_Z^{LE} and u_Z^{TE}, respectively, denote the vertical displacement of points located at the leading x^{LE} and the trailing edge x^{TE} of each wing section for which the twist angle is computed. Moreover, the fuselage rotation has been subtracted from the results given by Eq. (1), forcing the computed twist to be zero at the wing root section. It is worth remembering that the inclinometer used for controlling model angle of attack is located inside the fuselage. Therefore, the wing root incidence is a suitable reference value to compute twist. In other words, the angle of attack at the root is always set to the proper value, irrespective of the testing conditions, and so the fuselage rotation can be taken as zero. The second parameter under study is the vertical displacement of the wing (along the z axis). This value is provided mainly for reference purposes (it helps in depicting the wing deformed shape), as it is not so important from the point of view of aerodynamic interference (its effect in downwash is quite limited). The quarter-chord line is adopted as a reference for plotting the vertical displacements given its special importance in aerodynamics. The most relevant information obtained from the multiple analysis runs is presented in the next section. The displacements and rotations plotted haven been normalized using the maximum value obtained throughout the simulation campaign. Therefore, their absolute values are always contained inside the [0, 1] interval. As a reference, the maximum wing deflection was close to 10 mm and the maximum rotation was approximately 1°.

It should be noted that the deformations presented in this work are only due to aerodynamic forces, as the contribution of the model weight has not been accounted for. To evaluate the mechanical effect of the twin sting on wing deformation, a limited number of structural runs without booms (booms-off) have been performed. For these computations, the model displacement has been constrained by clamping the body–tail reference node (thus achieving an effect similar to a conventional fuselage-attached sting).

A. Effect of Sting Position on Wing Deformation

The wing vertical displacement and rotation computed for a freestream Mach number $M_\infty = 0.85$ are presented in Figs. 4 and 5. Note that the displacement pattern inboard of the wing–boom adaptors is reversed with respect to the situation when the model is supported at the fuselage. A downward reaction at the booms is needed to counteract the lift force acting on the test model; therefore, the root section rises relative to the boom area. Outboard from the stings, the usual behavior is recovered; i.e., the upward vertical deflection increases toward the wing tip.

Figure 5 shows that the twist angle steadily decreases from the root to the wing tip for the booms-off condition. This is to be expected, due to the positive sweep of the wing. The twin sting alters this behavior causing the twist angle to increase near the wing root. As the angle of attack increases, this trend becomes more pronounced. The absolute value of twist at the wing tip observed for the booms-on configuration is smaller than the value attained when the model is supported through the fuselage. This behavior can be explained as follows. When the angle of attack increases, the upward lift force
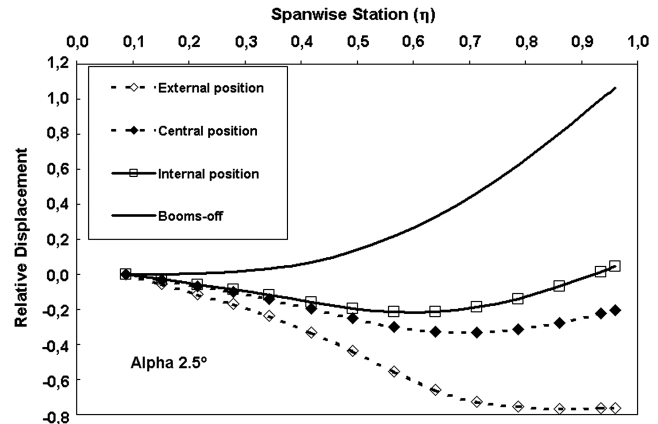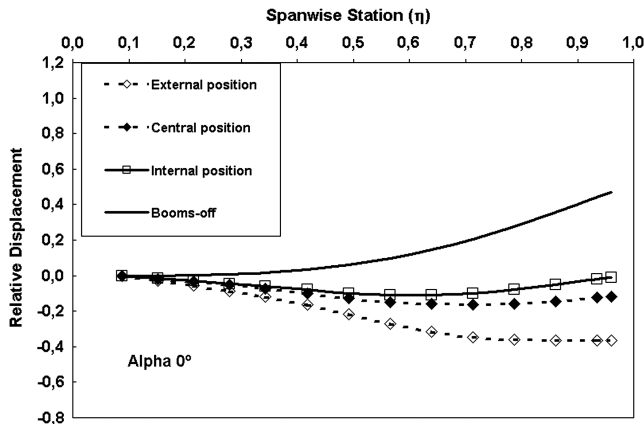

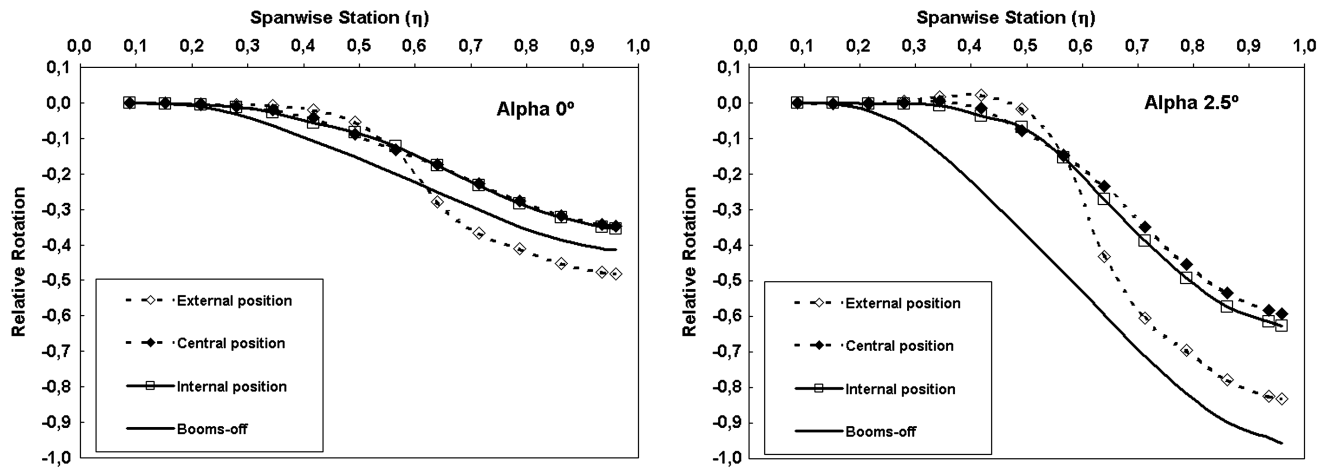**Fig. 4 Effect of support mechanism on wing deflection; $M_\infty = 0.85$, $\alpha = 0°$, and 2.5°.**

Fig. 5   Effect of support mechanism on wing twist; $M_\infty = 0.85$, $\alpha = 0°$, and 2.5°.

originated at the HTP grows, causing an additional nose-down (negative) moment on the fuselage. This pitch unbalance must be compensated by the sting booms, which react with an opposite torsion moment, producing a nose-up (positive) rotation of the wing sections inboard of the adaptors. On the other hand, due to the backward sweep of the wing, there is a coupling between bending deformation and rotations (with local angle of attack decreasing when the wing bends upward). Close to the wing root, the positive rotation due to the adaptor moment dominates, causing the twist angle to increase initially. In the area between the stings, the vertical displacement pattern is reversed, and so bending deformations do not lower the local angle of attack. Moving further outboard, the effect of boom torsion vanishes (the outer section of the wing is only subject to the aerodynamic loads with the adaptors having no effect) and the usual booms-off trend is recovered. Despite the important differences in the twist pattern, the overall wing rotation is reduced when using twin booms (except for the widest spacing at zero angle of attack, a situation in which deformations are small across the board anyway). The same can be said about the bending deflections, but in this case, the change is more dramatic, as the displacement field is completely reversed. It is important to keep in mind, however, that the vertical displacements are much less likely to have a negative impact on tail-force measurements than the changes in local angle of attack.

Regarding the effect of sting position, numerical calculations predict larger deflections when the supports are placed farther away from the symmetry plane. This was to be expected; on the other hand, the similarity of the behavior of the two smaller spacings is remarkable. In particular, regarding the twist distribution (Fig. 5), there is almost no difference between both configurations (the differences observed in the plot are probably within the margin of

error of the numerical model). This is due to the relative proximity of the two innermost adaptor positions and the large stiffness of the wing section near the root (where both chord and thickness are highest). Moving to the outermost sting position, a marked change of the curves is seen, with the reversed deformation pattern inboard of the boom becoming more pronounced. In this case, the wing is attached at a section of lower stiffness, farther apart from the symmetry plane and, consequently, the effects of torsion become apparent.

B.   Effect of the Angle of Attack

An increment of the angle of attack gives rise to a higher wing loading that, in turn, increases the vertical spanwise displacements. The local rotation angle is also affected in a similar way, though to a lesser degree. As explained before, this is due to the change in HTP lift (the test model is not trimmed), which causes a positive wing twist inboard of the adaptors. The behavior is more pronounced for the outer wing–boom adaptor position, as the part of the wing subject to this torsional loading spans a longer distance. Figure 6 shows the computed effects of the angle of attack for the outer sting position.

Observe that close to the wing root, the twist plots change very lightly, with the angle of attack reflecting the elevated stiffness of the wing. It is possible to observe at the spanwise station $\eta = 0.55$ that the rotation angle is insensitive to changes in the model incidence and remains almost constant. This reflects the change in support conditions between the different areas of the wing. Close to the fuselage, the effect of the booms is important; near the tip, the behavior is similar to the booms-off condition; and in between, there is a point at which a balance is achieved.
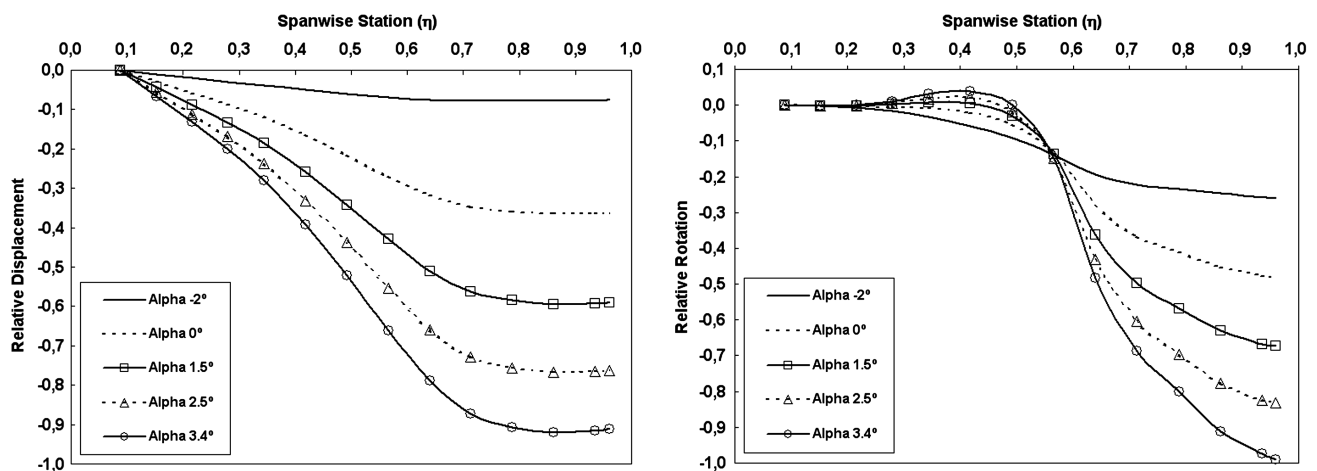

Fig. 6   Effects of the angle of attack on wing deformation, outermost boom position, and $M_\infty = 0.85$.
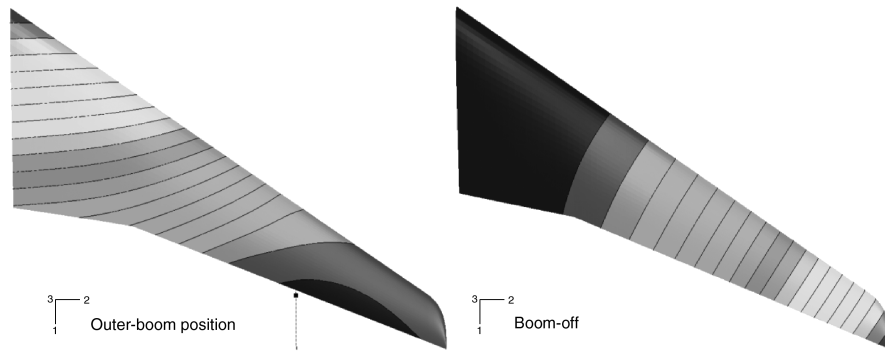
Fig. 7   Vertical displacement contours on the wing; $M_\infty = 0.85$ and $\alpha = 2.5$.

C.   Global Effects of the Twin-Sting Support on Wing Deformation

With the aim of giving a better understanding of the effects of the twin sting on the wing, its deformed shape is drawn for both the booms-on and booms-off configurations (Fig. 7). The differences on the isodisplacement lines computed for both cases are quite apparent.

For the booms-off configuration, the displacement isolines are approximately perpendicular to the midchord line (more precisely, to the elastic axis of the wing). However, when the sting is attached to the wing, the displacement pattern is vastly different.

Notice that near the wing root, the lines are perpendicular to the fuselage, which indicates that the displacement field corresponds approximately to a rigid-body rotation of the fuselage. Part of this motion is due to bending of the booms (which causes a rigid-body displacement of the complete model, wings included). There is also a contribution arising from wing torsional deformation between the fuselage and the sting. This can be evidenced by comparing the distance between the isodisplacement contours at the root and boom sections. The spacing between the curves being wider at the sting position means that the wing root section is pitching upward with respect to the boom area. Remember once again that the pitch sensing device that controls the test-model attitude is located inside the fuselage, and so the rigid-body displacements of the complete model do not have any affect on the measurements. Therefore, only the torsional deformation has to be accounted for as a true aeroelastic effect.

Halfway between the fuselage and the boom, the lines curve toward the leading edge, creating a motive that is somewhat reminiscent of the free-wing configuration. However, once the wing–boom adaptor area is reached, the deformation pattern changes abruptly. The boom stiffness restricts the rotation of the wing sections, and the vertical displacement field over the outboard wing region becomes almost constant.

Another interesting result from the graphs is that whereas the displacement field is completely reversed with respect to the booms-off situation (i.e., the wing bends downward instead of upward), the same is not true for the twist distribution (Figs. 4 and 5). Positive twist angles are only obtained for the widest spacing, and even in that case, they are small compared with the negative rotations that occur on the outboard part of the wing (Fig. 5). The cause is the large pitch-up moment introduced by the HTP for moderate values of the fuselage incidence. When the model attitude is close to horizontal, there is a net downward force acting on the HTP (the test model is not trimmed) that causes the boom section to rotate downward with respect to wing root. This negative twist is partially countered by the positive contribution due to bending (as the wing deflection distribution inboard of the adaptor is reversed, the effect of the wing sweep is to increase the local angle of attack). The two competing effects (torsion and bending) partially cancel each other, resulting in a very flat twist plot inboard of the wing–boom adaptors (Fig. 6 illustrates this behavior). Once the angle of attack is increased, the tail downward force is reduced, whereas the positive twist due to wing bending increases as a result of a higher wing load. The twist reversal phenomenon is therefore most pronounced at high incidence settings: in fact, it disappears when the angle of attack is negative (see Fig. 6).

V.   Conclusions

It has been shown that the *one-way* coupling procedure developed seems to be adequate for assessing the wing aeroelastic behavior in the frame of these particular research activities. Direct measurements in a cryogenic test environment corroborate the accuracy of the results. It is important to stress that the dynamic pressure expected during cryogenic-tunnel entries is higher than (about three times as large as) the value encountered during conventional testing (which is the subject of this study). If the results are accurate in a situation in which large deformations are produced due to high-pressure loading, it seems very reasonable to expect an even better agreement under less severe conditions. What is more, in the vast majority of cases, the net effect of twist deformations is to reduce the local angle of attack; thus, the geometric changes on the real test model are not expected to be larger than those predicted here (wing load is reduced, due to the deformation). Hence, the deformations calculated can be considered as a realistic bound of the real ones.

In the past, there has been an important level of uncertainty associated with twin-sting testing. It was speculated that the reduction in aerodynamic interference at the tail could be offset by large changes in downwash caused by increased wing twist. This study has proven these suspicions to be unfounded (within the range of parameters covered). The global deformations due to the twin-sting mounting system are not higher than those expected when a conventional single-sting support system is employed (booms-off configuration). The fact that the deformation pattern tends to reverse inboard of the booms causes the average displacements to become smaller (the effects occurring inboard and outboard of the adaptors tend to cancel each other). This holds true even for the largest boom spacing, showing that there is much greater freedom in choosing the optimum separation (for aerodynamic purposes) than was previously thought possible.

On the negative side, it is apparent that the shape of the twist distributions is vastly different from the booms-off case. This negates the possibility to reproduce the aeroelastic response of the free aircraft over a wide range of flight conditions. This is further complicated because the deformation field depends not only on boom position and model angle of attack, but also on HTP incidence setting. Therefore, the shape of the model would have to be tailored carefully for specific test conditions if aeroelastic similarity is to be achieved. In particular, it is problematic to test the same model using both single- and twin-sting mounting. These negative findings are partially offset by the fact that the actual values of the displacements are smaller when using twin stings.

Acknowledgments

References

[1] Piat, J. F., and Steve, N., "Recent Experiments with New Twin-Debs-Sting Supports in Onera's Large Wind Tunnels," AIAA Paper 2002-2921, 2002.

[2] Lyonnet, M., Piat, J. F., and Roux, B., "Model Support Interference Assessment Using a Metric Rear Fuselage and a Twin-Sting at ONERA S2MA Windtunnel," *Proceedings of the ICEF 1994 Conference*, ONERA, TP 1994-125 E, Turin, Italy, 1994.

[3] Quest, J., and Wright, M., "Investigation of a Modern Transonic Transport Aircraft Configuration over a Large Range of Reynolds Numbers," AIAA Paper 2002-0422, 2002.

[4] Gross, N., "ETW Analytical Approach to Assess the Wing Twist of Pressure Plotted Wind Tunnel Models," AIAA Paper 2002-0310, 2002.

[5] Luo, H., , Baum, J. D., and Löhner, R., "Edge-Based Finite Element Scheme for the Euler Equations," *AIAA Journal*, Vol. 32, No. 6, 1994, pp. 1183–1190.
doi:10.2514/3.12118

[6] Roe, P. L., "Approximate Riemann Solvers, Parameter Vectors and Difference Schemes," *Journal of Computational Physics*, Vol. 43, No. 2, Oct. 1981, pp. 357–372.
doi:10.1016/0021-9991(81)90128-5

[7] Van Leer, B., "Towards the Ultimate Conservative Difference Scheme 5: A Second Order Sequel to Godunov's Method," *Journal of Computational Physics*, Vol. 32, No. 1,1979, pp. 101–136.
doi:10.1016/0021-9991(79)90145-1

[8] Löhner, R., *Applied CFD Techniques*, Wiley, New York, 2001.

[9] Zienkiewicz, O., and Taylor, R., *The Finite Element Method*, 5th ed., Vol. 1, Butterworth-Heinemann, Oxford, 2000.

[10] Joldes, G. R., Wittek, A., and Miller, K., "An Efficient Hourglass Control Implementation for the Uniform Strain Hexahedron Using the Total Lagrangian Formulation," *Communications in Numerical Methods in Engineering*, Vol. 24, No. 11, 2007, pp. 1315–1323.
doi:10.1002/cnm.1034

[11] Walter, U., *ETW User Guide*, ETW GmbH, Rept. ETW/D/95001/A, Cologne, Germany, Jan. 2004, http://www.etw.de/pdfs/ETW_USER_GUIDE.pdf [retrieved 4 Feb. 2010].

[12] Ruyten Sellers, M. E., "Demonstration of Optical Wing Deformation Measurements at the Arnold Engineering Development Center," AIAA Paper 2009-1520, 2009.